IJME

Int. J. of Applied Mechanics and Engineering, 2025, vol.30, No.1, pp.101-111
DOI: 10.59441/ijame/195997

EVALUATION OF MICROSTRUCTURE AND MECHANICAL PROPERTIES RESULTING FROM GAS NITRIDING PROCESS FOR DIFFERENT TYPES OF STEEL

Faras Q. Mohammed*
Production Engineering and Metallurgy Department, University of Technology, Baghdad, IRAQ
E-mail: firas.q.mohammed@uotechnology.edu.iq

Ibrahim Abd L-Kareem Ahmed
Company for Steel Industries, Ministry of Industry and Minerals, Baghdad, IRAQ

Sameer Khalaf Fyayyadh
Department of Engineering Machine and Agriculture Equipment, College of Agricultural Engineering Sciences, University of Baghdad, IRAQ

This work investigates the effect of the gas nitriding process on the surface layer microstructure and mechanical properties for steel 37, tool steel X155CrVMo12-1 and stainless steel 316L. Nitriding was conducted at a temperature of *550°C* for 2 hours during the first stage and at *750°C* for 4 hours during the second stage. SEM and X-ray diffraction tests were performed to evaluate the microstructural features and the major phases formed after surface treatment. SEM and X-ray diffraction tests were performed to assess the microstructural features and the primary phases formed after surface treatment. The new secondary precipitates were identified as γ′-Fe4N, ε (Fe2–3N), and α-Fe, exhibiting an uneven chain-like pattern within columnar grains. A significant increase in the nitride layer thickness (*34.4 μm*) was achieved for X155 compared to AISI 316L and steel 37. Also, Gas nitriding caused a significant increase in hardness at the first stage for X 155 tool steel and AISI316L steel with hardness percentage enhancement of *0.87%* (*655HV*) and *0.28%* (*219HV*) respectively, while for steel 37 samples the hardness reached its maximum value of *340 HV* for the second nitriding stage with hardness percentage enhancement of *0.78%*. There was no significant improvement in surface hardness after second nitriding stages for X155 and AISI 316L steels. The effects of time and gas flow rate during the process were particularly evident on hardness values, especially after the first stage.

Key words: AISI 316L, gas nitriding, micro-hardness, steel 37, X155.

1. Introduction

It is well known that various types of steel serve as a significant resource for numerous engineering applications that demand high mechanical properties to withstand working conditions relevant to the application. Tool steel can be hardened and tempered under specific conditions, enabling it to cut, shape, form, and blank at both low and elevated temperatures [1]. Conversely, marine applications and tools that interact with solvents, chemical solutions, and steam boilers in power plants underscore the necessity of using stainless steel [2]. Another type used in construction and certain applications requiring high ductility can be characterized as mild steel [3]. Cold work tool steel DIN (1.2379) is regarded as a preferred material for applications that demand high hardenability, good wear resistance, and high softening resistance [4, 5]. Austenitic stainless steel 316L has extensive industrial applications due to its high corrosion resistance. It possesses a remarkable ability to be utilized in various extremely corrosive industries, thanks to its excellent corrosion resistance derived from the high content of chromium and nickel, which facilitates the formation of

* To whom correspondence should be addressed

a stable and passive surface oxide layer [6, 7]. However, these soft steels have low hardness and poor wear resistance. Accordingly, their use is still limited to low and moderate resistance to abrasion and hardness applications [8]. In terms of tool steels, they are exceptionally tough materials; however, their wear resistance is relatively low, which restricts their use in low-speed machining. This creates a trade-off between toughness and wear resistance, limiting the application of these super hard tools to lighter cutting speeds [9]. In summary, these types of steel encompass a broad range of industrial and construction applications, for which demand has significantly increased.

Many researchers have applied surface treatments to modify and enhance the material's surface to improve its contact with the atmosphere [10-12]. Nitriding is a well-established diffusion-based thermo-chemical surface treatment widely used in the industry [13, 14]. In most applications, the primary goal is to increase surface hardness and develop wear resistance. It is favored in various engineering sectors due to its effectiveness with minimal distortion. Nitriding is extensively utilized as a surface process in tooling manufacturing industries. Researchers have extensively studied this process, resulting in a significant increase in surface hardness and the formation of compressive residual stresses [15-17]. The diffusion of nitrogen into the material's surface during this treatment creates a unique microstructure that greatly enhances physical and chemical properties [18]. Nitriding can be categorized into three main types: gas nitriding [19, 20], salt bath [21] and plasma nitriding [22]. Numerous nitriding systems are commercially available to facilitate the introduction of atomic nitrogen in liquid, controlled gas, or plasma environments [23, 24]. GN, or gas nitriding, is achieved by introducing atomic nitrogen into the metal surface at temperatures between *495°C* and *565°C*. In contrast, the fluidized bed nitriding (FBN) process is typically conducted in a fluidized controlled environment furnace with the presence of ammonia gas [25, 26]. Most recent research has focused on this treatment to enhance surface properties by controlling the nitriding parameters and demonstrating their effects primarily on wear properties.

The aim of this research is to present a new investigation into the surface nitriding gas treatment of carbon steel, tool steels and stainless steels with a comprehensive evaluation of the microstructure and mechanical properties resulting from this treatment. These types of steels fall within a wide range of industrial and construction applications, for which the demand has increased greatly in recent times specially for the steel casting molds Industries, which includes various specializations, starting with the production of different types of steel and extending to the manufacturing of steel structures for electrical transmission towers, as well as factories for hot and cold forming molds that must withstand the stresses resulting from the forming processes.

2. Materials and methods

The alloys used in this study are steel 37, tool steel X155CrVMo12-1 and stainless steel 316L, with chemical compositions shown in Tab.1. These specimens were received with dimensions of $20\times100\times20$ *mm.* Before the nitriding process, a mechanical grinding for all samples was performed by using the emery paper of *240* grits and then rinsed with acetone. After grinding the samples were ultrasonically cleaned in ethanol for *15 min* prior to the nitriding process. This will helps to reduce or remove the oxide layer that exist on the substrate surface which acts as barrier for nitrogen diffusion thereby nitride formation.

Surface treatment was achieved by using a hot wall chemical vapor deposition system (HWCVD), which consists of high temperature precision bench-top vacuum tube furnace type GSL-1600-60X, consisting of *60 mm* diameter high purity Alumina tube of *54 mm* inner diameter and *1000 mm* length, using $MoSi_2$ as heating elements. The temperature of GSL 1600-60X tubing furnace is controlled by high precision SCR power controller with accuracy ±°*C*, 51 segments that are programmable up to*1600°C* and installed with stainless steel vacuum sealed flange. The furnace is equipped with a double step rotary vacuum pump of *120* SLPM (standard litters per minute) capacity assembled with a sensitive pressure senor (needle vacuum gauge) [1, 8]. The nitriding process was performed with a gas mixture of $2N_2{:}1NH_3$ by using of ammonia (NH_3) as a reactive gas at a relatively high deposition temperature in the (HWCVD). The nitriding process was accomplished in two stages. The first nitriding stage was performed at *550°C* for *2 hr*. with gas flow rate $5\ cm^3\ /\ min$, while the second nitriding stage was achieved at *750°C* for *4 hr*. with gas flow rate $2.5\ cm^3\ /\ min$. The corresponding

tool steel, stainless steel and carbon steel treated samples are coded as T, S, C, respectively. The microstructure was examined with scanning electron microscopy (SEM) type Tescan VEGA 3SB with accelerating voltage *200-30 kV* to determine the nitriding layers presented phases. The X-Ray diffraction was performed using an XRD-6000 Shimadzu X-ray diffractometer with Cu-Kα radiation and incident angle of *0.154 nm*, and voltage of *40.0 kV*, current of *30.0 mA*, the step size was *0.0500 deg*., with angular range of $2\theta = 10 \div 80$ (degree) and count time : *0.30 sec*. LCCD cards for diffraction data were used for characterizations of X-ray diffraction to analyze phases for each nitriding layer. Before the microstructure analyzing, the nitrided samples were chemically etched using a chemical solution of *20 ml* HCL+ *20 ml* HNO_3 + *20 ml* acetic acid + 4 drops glycerol to reveal the nitride layer.

The Vickers micro-hardness (HV) test was performed for the two stages of nitriding on the treated zone using the Vickers micro hardness tester– South Korea device model with a major load of *0.98 N*. The samples for the phase characterization (XRD) and structural morphology (SEM), had the dimensions of $20 \times 20 \times 10\,mm$ for the thickness, width and length respectively.

Table 1. Composition of investigated steels (Wt %)[6].

Elements	C	Si	Mn	Cr	Ni	Mo	V	S	P
Steel 37	*0.18*	*0.35*	*0.28*	*0.031*	*0.067*	*0.0011*	-	*0.05*	*0.04*
X155CrVMo12	*1.48*	*0.32*	*0.24*	*10.74*	*0.18*	*0.76*	*0.83*	*0.03*	*0.02*
AISI 316L	*0.011*	*0.45*	*0.38*	*17.2*	*11.4*	*1.5*	-	-	-

3. Results and discussion

Figure 1 presents the XRD pattern analysis of the three proposed nitride steel sheets treated by the second stage of the gas nitriding process. Generally, the XRD patterns indicate that the second stage of nitridation does not result in significant changes in the types of phases produced for each type of steel used. The primary difference observed was after the application of the second stage of nitridation, which led to an increase in the thickness of the nitriding layers due to elevated deposition temperatures and gas flow rates. Additionally, a development in the crystalline structure of the presented phases was noted for the second stage nitrided samples, resulting in more crystallite phases with higher diffraction intensity and more shifted diffraction angles compared to the first stage of nitriding. In all XRD patterns, the as-received samples exhibited only the (101) α-Fe peak at a *44.71* 2θ angle and the (200) α-Fe peak at a *64.94* 2θ angle. Conversely, the XRD patterns of the nitrided samples displayed several peaks that differed from those of the as-received samples due to the effects of the nitriding process. The peaks observed in the treated samples varied from one another due to differences in the chemical compositions of the samples. For the 316L steels, the XRD pattern exhibited weak γ'-Fe_4N peaks alongside strong α-Fe peaks. Additionally, the diffraction patterns of the treated 316L steel samples indicated that the γN phase (noted at 2θ angles of 37.4, *43.1*, and *53.6* with indices of (101), (111), (200), respectively) is the predominant phase in these substrates. In contrast, the main phase present in the modified layer is the metastable phase, known as the supersaturated or 'expanded' austenite phase. Moreover, there was shifting to lower angles for the austenite peaks in the second-stage nitrided samples which can be attributed to the residual compressive stresses that was introduces in the surface nitriding layer. The shifts in γN peaks are linked with the highest content of nitrogen in this nitrided samples. For steel 37 samples, it can be clearly observed that the expanded austenite substrate peaks cannot be found for these samples as the thick γN was presented on these substrates. It is important to note here that other preferable phases can be observed in the pattern of steel 37. The C_3N_4 phase was detected at 2θ angles *28.39*, *37.13*, and *72.43* with (100), (110), and (112) indices, respectively. Also, strong peaks for the expanded γFe_2N -austenite were distinguished at *42.5*, *53.217*, and *74.259* with (102), (121), and (141) indices, respectively.

For treated X155 steel substrates, various phases were also recorded. Nitride peaks corresponding to chromium nitrides (CrN), ε (Fe_2–3N), γ' (Fe_4N) and C_3N_4 phases were detected on the X155 steel nitrided surfaces. For X155 nitrided steel, the significant shifting and broadening were attained for austenite peaks as a result of the nitrogen supersaturating and expanded austenite γN in the lattice. In contrast, the austenite (γN) expanded (200) planes found to be more widely spaced comparing to other planes in XRD pattern, which indicates the occurrence of a deviation from the cubic FCC unit cell for these patterns.

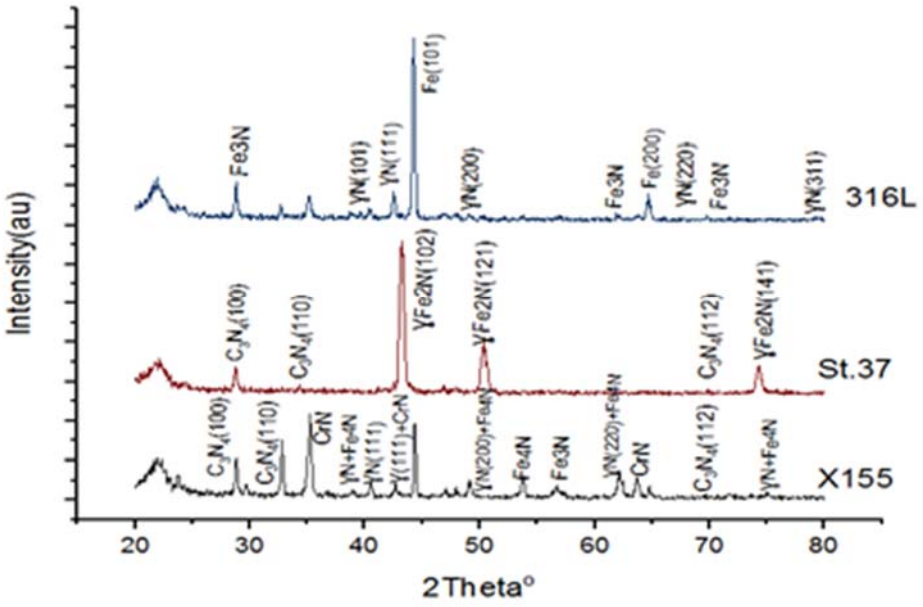

Fig.1. XRD patterns of the different steel sheets treated by second stage gas nitriding process.

Metallographic investigations were performed by using scanning electron microscope (SEM). In general, this test displayed that the main microstructural feature for all treated steel samples consists of compound layer with higher nitrogen concentration. In tool steel, these nitride compounds exist as FCC Fe_4N, designed as (Ý), and hexagonal Fe_{2-4}, designed as (ε) [27]. For 316L steel (Fig.2), the compound layer (white layer), diffusion zone, and core (matrix) consists of an internal tempered martensitic matrix and a nitride layer on the external surface. The existence of white lines (uneven chain-like pattern) indicates the iron nitrides formation ($Fe_{3-4}N$) on the nitrided surface [28]. The nitride layer consists of a nitrogen diffusion zone where fine nitride plates precipitate and a compound layer formed on the outer part. For steel 37 (Fig.3), the homogenous precipitation of nitrides occurs by a continuous and simultaneous clustering of both interstitial (N) and substitutional (Cr, V, Mo) solutes and a final transformation of the ordered clusters into equilibrium nitrides [16]. The tempered martensitic matrix contains a typical alloy carbide, with the core being relatively softer than the surface. This presents an advantage for steel, as it exhibits greater toughness compared to a pure martensitic matrix under any loading conditions. It is widely recognized that a martensitic matrix is hard and brittle, with insufficient plastic deformation capacity for many industrial applications [29]. Nitrogen can diffuse more rapidly in areas near the surface, while the diffusion rate significantly decreases further from the surface [30]. Results show that the compound layer contains a higher concentration of nitrogen than the diffusion zone. This phenomenon is well-documented, as nitrogen atoms supersaturate the layer due to the nitriding process. For X155 steel, Fig.4 illustrates the formation of chromium nitride alongside the iron nitride phase, as indicated by XRD analyses (Fig.1). The alloying elements exhibit varying degrees of affinity for nitrogen, with the formation of chromium nitride being thermodynamically more stable. These carbides play a crucial role in enhancing the hardness of both the compound layer and the diffusion zone. It is important to note that the type, distribution, and quantity of the nitride phases directly influence the surface properties.

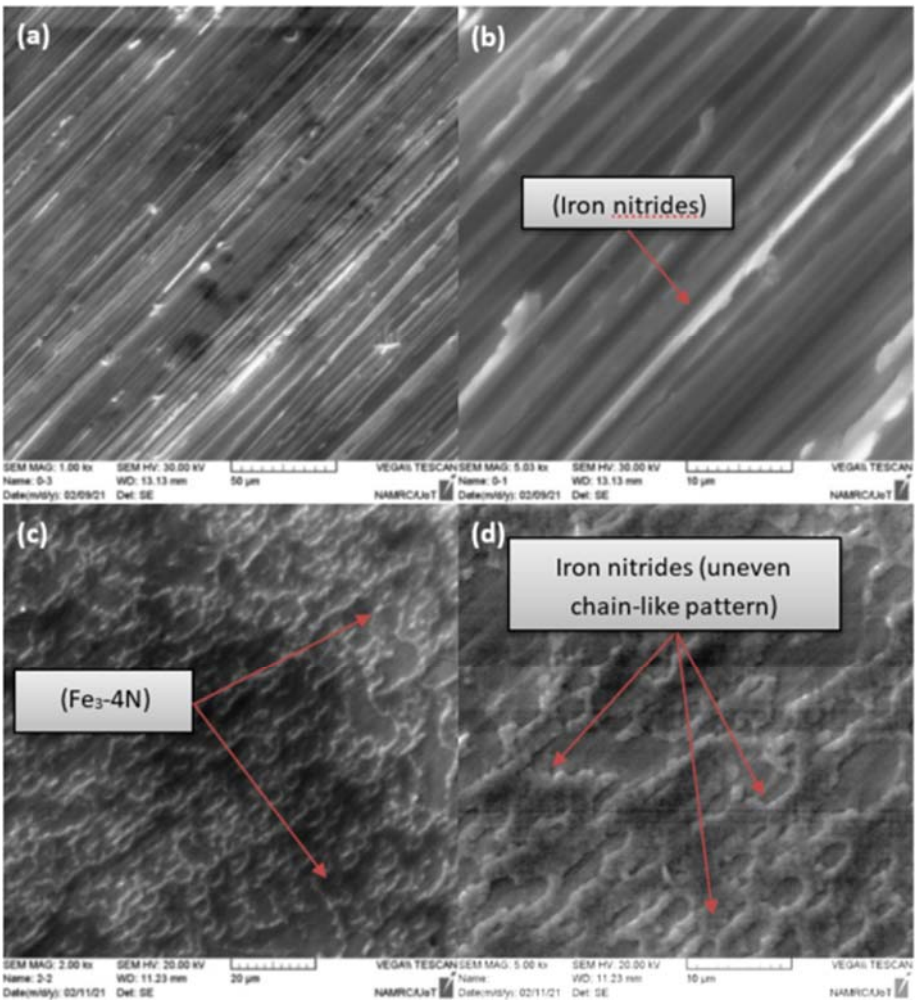

Fig.2. Scanning electron photographs of 316L stainless steel in low magnification (left) and high magnification (right) for one stage of nitriding (a, and b), and two stages of nitriding (c, and d).

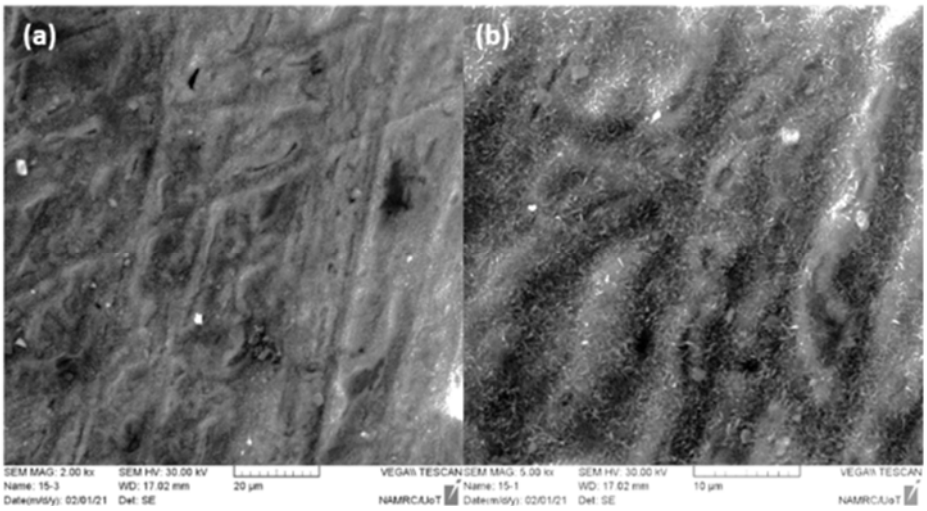

Fig.3. Scanning electron photographs of carbon steel 37 in low magnification (left) and high magnification (right) for one stage of nitriding (a and b), and two stages of nitriding (c and d).

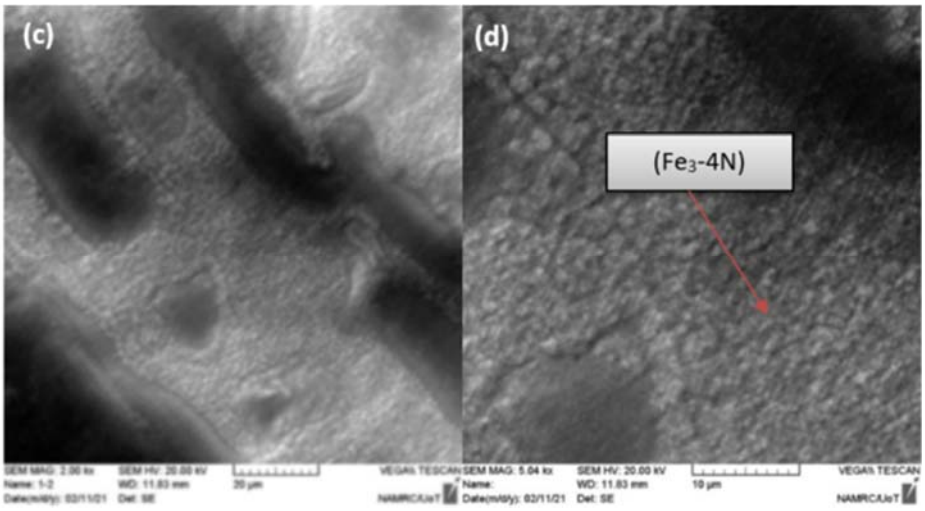

Fig.3 cont. Scanning electron photographs of carbon steel 37 in low magnification (left) and high magnification (right) for one stage of nitriding (a and b), and two stages of nitriding (c and d).

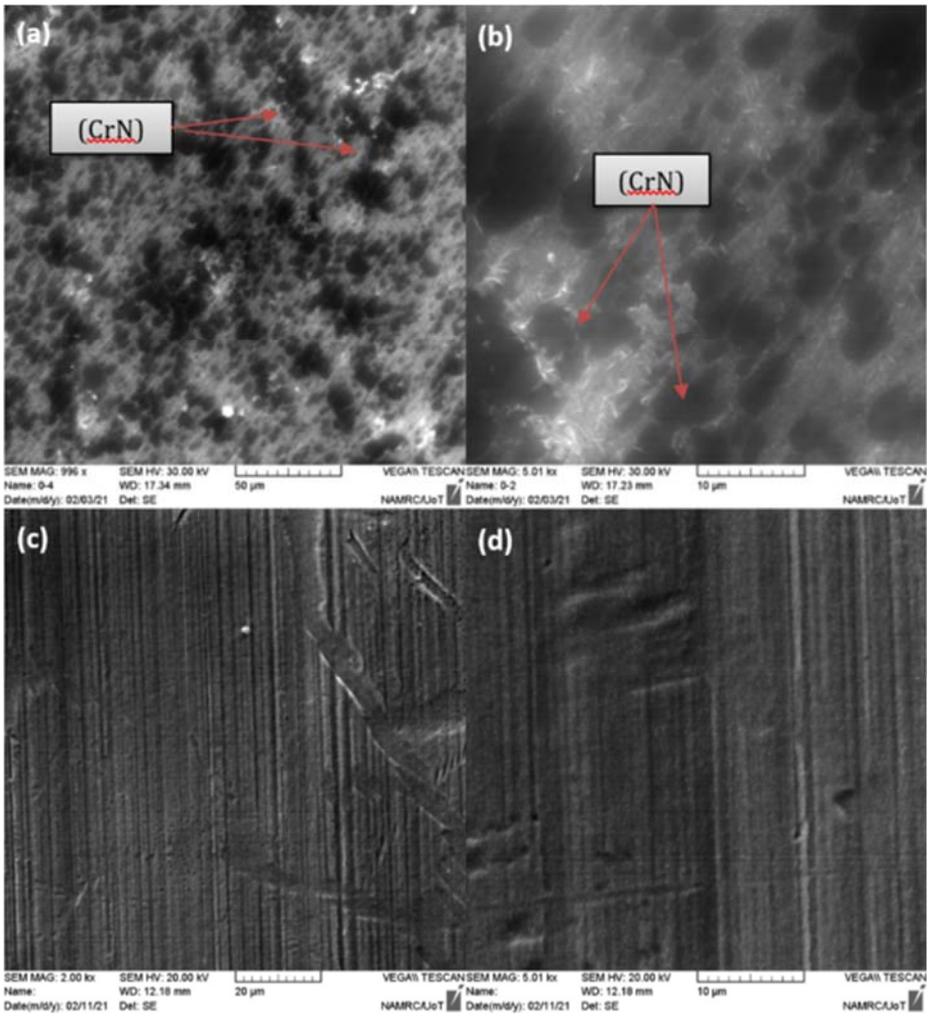

Fig.4. Scanning electron photographs of tool steel in low magnification (left) and high magnification (right) for one stage of nitriding (a and b), and two stages of nitriding (c and d).

Figure 5 illustrates SEM images of the cross-sectional view of the compound layers deposited on the examined steel substrates. The thickness of the formed layers was *34.4* µ*m*, *9.3* µ*m*, and *4.7* µ*m* for X155, 316L, and steel 37, respectively. This variation in thickness values may be attributed to the surface response of the different steel substrates to the nitriding, even though the treatment was conducted under the same conditions. Among the three steel substrates, the nitride layer on the X155 substrate exhibits a greater thickness. This can be attributed to the effectiveness of the chemical composition in these steel alloys, which have a high concentration of alloying elements that promote the formation of nitrides with a greater layer thickness. It is important to note that the nitration was conducted at higher temperatures, which may enhance energy, increase molecular movement, and consequently, the diffusion rate. It can be concluded that the thicker layer obtained for X155 substrates is due to the higher nitrogen solubility of their austenitic structure, even at a low diffusion rate.

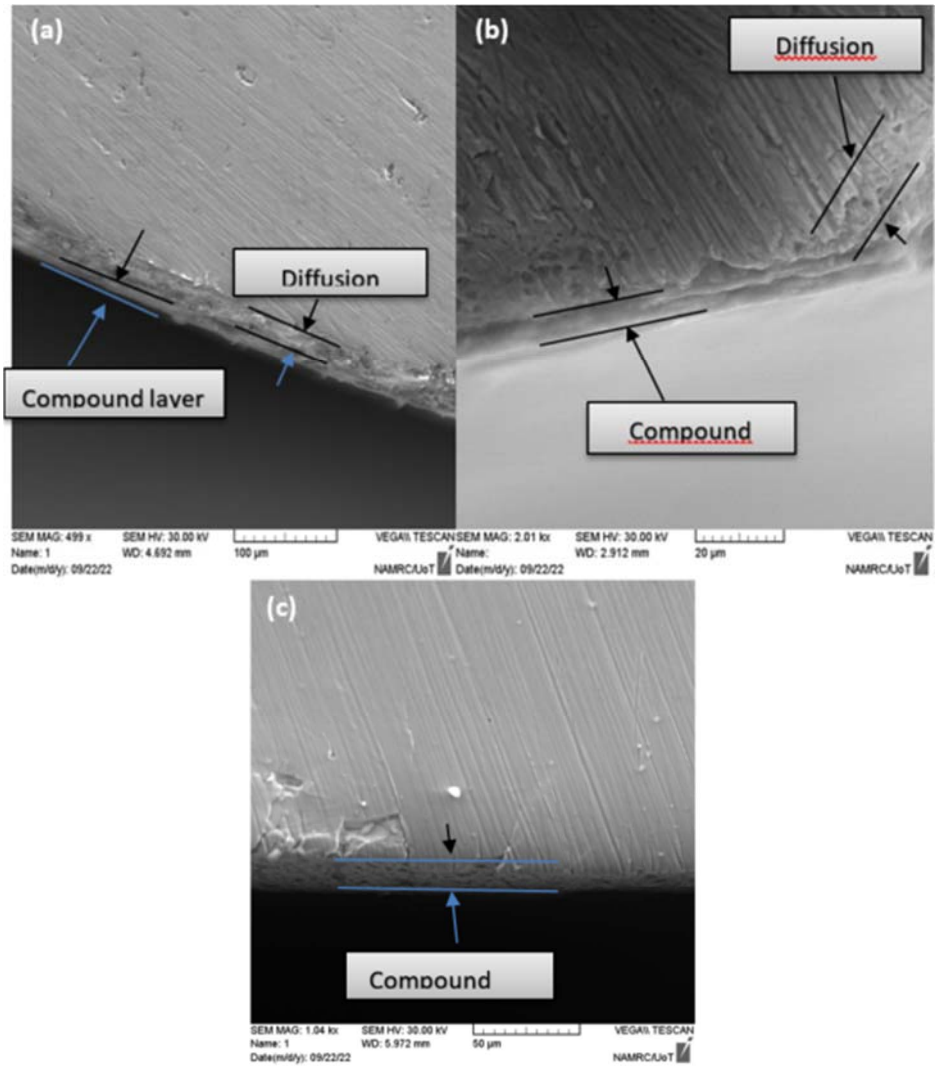

Fig.5. Cross-sectional view of different layers obtained by second stage gas nitriding process on:
(a) X155 ,(b) steel 37 and (c) AISI 316L.

Surface treatments are typically applied to enhance the hardness of the surface and subsequently improve the wear resistance of steel alloys. Alloying elements such as Mo, Cr, Ti, and V are particularly effective in forming nitrides in various morphologies. These nitrides precipitate as thin discs on the cube planes

of the α-Fe matrix. Both interstitial and substitutional atoms on the cube planes generate significant elastic strain due to the mixed clusters, which may lead to an increase in the hardness of the nitride layers in steel. If the process atmosphere is not controlled, decarburization will inevitably occur. This is an undesirable phenomenon that negatively affects the surface properties. However, nitriding can produce a homogeneous and hard layer of a specific thickness on the treated surface [2]. Higher hardness values were recorded for treated X155 substrates (*655 HV* for one-stage nitriding and *306 HV* for two-stage nitriding), as shown in Tab.2. These hardness results demonstrate that the one-stage process has a more significant impact on mechanical properties than the two-stage process for the X155 and 316L steels.

Hardness variation measurements for the untreated and treated samples were also obtained as a function of distance from surface for the experimental steels (Fig.6(a-c)), where the micro-hardness values are measured diagonally from one edge to another; and the test line's length is *250* μm moving the hardness test zone towards the centre of the sample. The hardness decreases significantly, as its clearly observed that the outer surface and diffusion zone have stable nitride phases, which can be clarify why the hardness was found to be higher than the tempered martensitic matrix at the centre of the samples. For X155 steel the hardness of not nitride sample was found to be *350 HV*. The higher hardness values were recorded for treated X155 substrates (*655 HV* at one-stage nitriding and *368 HV* at two-stage nitriding) with hardness percentage enhancement of *0.87%* and *0.02%* for the first and second nitriding stage respectively. as shown in Tab.2. These hardness results prove that the one-stage process has a greater impact on the mechanical properties than the effect of the two-stage process. At the first stage, the nitrogen atoms with a high flow rate either dissolved in the ferrite phase at the diffusion zone or interact with alloying elements to produce nitrides precipitations. Hence, the strengthening resulting from the dispersion of nitrogen atoms with precipitates could cause a significant increase in surface hardness, as in second stage the reactions between the ferrite and nitrogen gas stop, and extending the nitriding time is not as beneficial for the process as recorded by other authors [31]. The hardness variations for steel AISI 316L indicate the same effect associated with the conditions of nitriding stages (*172 HV* for not nitrided sample). In this sample the hardness records *228 HV* and *196 HV* for the first and second nitriding stages respectively, with hardness percentage enhancement of *0.325%* and *0.139%* respectively. The main reason for the decrease in hardness in the second stage of the nitration process may be attributed to the precipitating of chromium carbides, known as chromium depletion, at the grain boundaries during the nitriding process. This precipitation happens because the carbides are insoluble at a temperature range of $550 \div 850$ *°C*. The removal of chromium atoms along the grain boundaries of stainless steel resulted from sensitization [32]. Also, it should be noted that with the increase in temperature, the base metal's ductility increases due to recrystallization and the removal of internal stresses, in addition to the increased movement of dislocations, which leads to a decrease in the resistance of the metal to external stresses. The only exception for hardness increases with nitriding time was found for steel 37 samples, where in steel 37 expanding the nitriding time considered to provide the greatest hardness results. As these samples show moderated hardness of *190 HV* for not nitride surface, the hardness increased as the nitriding time increased from *258 HV* for the first stage till it reached its maximum value of *340 HV* for the second nitriding stage with hardness percentage enhancement of *0.35%* and *0.78%* respectively. This enhancement can be attributed to the combined effect of nitriding process and martensitic transformation that can be accord for this samples as it was also recorded by other authors [31].

Table 2. Surface hardness of steel substrates treated by one- and two-stages nitriding process.

material	initial hardness *HV*	first stage hardness *HV*	hardness percentage enhancement %	second stage hardness *HV*	hardness percentage enhancement %
X155CrVMo12-1	*350*	*655*	*0.87*	*368*	*0.02*
stainless steel 316L	*172*	*228*	*0.325*	*196*	*0.139*
steel 37	*190*	*258*	*0.35*	*340*	*0.78*

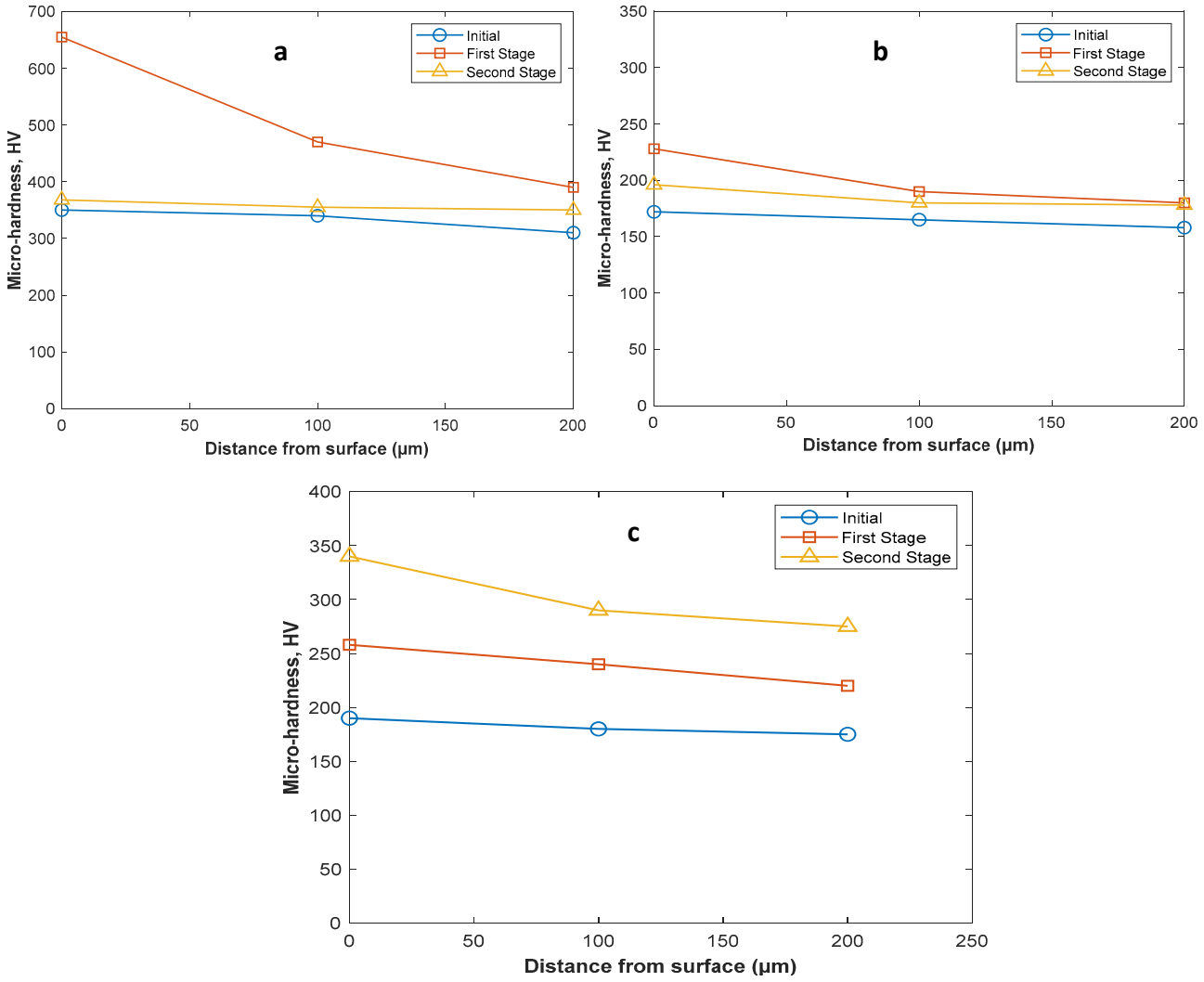

Fig.6. Micro-hardness profiles for nitride steel substrates after first and second stage gas nitriding process: (a) X155, (b) AISI 316L, and (c) steel 37.

4. Conclusions

The gas nitriding process for different steel alloys was performed, and the major goal was to find out the response of these alloys to the same variables of gas nitriding process. Based on the obtained results, a number of conclusions can be mentioned as follows:

- X-ray diffraction proved that the second stage of nitridation produced more crystallite phases with higher diffraction intensity and more shifted diffraction angles, with ε and Ý phases.
- After the second-stage of gas nitriding treatment, a thicker layer on the surface of X155 substrate was created, while a thinner layer was obtained for steel 37 and AISI 316L substrates.
- The effect of alloying elements of investigated kinds of steel on the nitriding efficiency was evident since high chromium content promoted the formation of thicker nitride layers by precipitation of carbides through the surface treatment.
- Gas nitriding caused a significant increase in hardness at the first stage for X155 tool steel and AISI316L steel with hardness percentage enhancement of *0.87*% (*655 HV*) and *0.28*% (*219 HV*)

respectively. After that, it started to decline reaching its lowest value of *360 HV* for X155 and *175 HV* for 316L which are very close value to the initial value before the gas nitriding operation began.

- An exception was found for steel 37 samples, where the hardness reached its maximum value of *340 HV* for the second nitriding stage with hardness percentage enhancement of *0.78%*. This enhancement can be attributed to the combined effect of nitriding process and martensitic transformation that taking place for these samples.
- An important relationship was found in this work for X155 and 316L steels that links the nitriding surface hardness with process time and gas flow rate, by which, short time and higher gas flow rate during first stage nitriding produced higher surface hardness; nevertheless, the longer time and reduced gas flow rate at second stage led to a decrease in the recorded hardness values.

Acknowledgements

The authors would like to thank the University of Technology in Baghdad, Iraq, and the State Company for Steel Industries for their support during this scientific work.

Nomenclature

C – high carbon steel/ steel 37
T – X155CrVMo/ tool steel
S – 316L steel /austenitic stainless steel
SEM – scanning electron microscopy
XRD – X-ray diffraction
SLPM – standard liter per minute

References

[1] Thamir A.D., Haider A.J. and Mohammed F.Q. (2017): *Titanium-base nanostructure coatings for AISI M52 tool steel by gas-phase mix process*.– Engineering and Technology Journal, vol.35, No.3, Part A, pp.181-190.

[2] Biehler J., Hoche H. and Oechsner M. (2017): *Corrosion properties of polished and shot-peened austenitic stainless steel 304L and 316L with and without plasma nitriding*.– Surf. Coatings Technol., vol.313, pp.40-46, doi: https://doi.org/10.1016/j.surfcoat.2017.01.050.

[3] Cho K.T., Song K., Oh S.H., Lee Y.K. and Lee W.B. (2014): *Enhanced surface hardening of AISI D2 steel by atomic attrition during ion nitriding*.– Surface and Coatings Technology, vol.25, pp.115-121.

[4] Hubbard P., Partridge J.G., Doyle E.D., Mcculloch D.G., Taylor M.B. and Dowey S.J. (2010): *Investigation of nitrogen mass transfer within an industrial plasma nitriding system I: the role of surface deposits*.– Surf. Coat. Technol., vol.204, pp.1145-1150, http:// dx.doi.org/10.1016/j.surfcoat.2009.08.029.

[5] Knerr C.H., Rose T.C. and Filkowski J.H. (1991): *Gas Nitriding of Steels*.– ASM Handbook, vol.4, ASM International, pp.867-881.

[6] *Properties and Selection Irons, Steels and High-performance Alloys*.– vol.1, 10th ed., Ohio, ASM Metals Handbook, 2005.

[7] Davis J.R. (1994): *Stainless Steels*.– ASM specialty handbook, ASM International, USA.

[8] Uhríčik M., Palček P., Hudecová S., Šurdová Z., Slezák M. and Chvalníková V. (2024): *The influence of heat treatment on the nitriding layer on austenitic steel*.– Journal of Physics: Conference Series, IOP Publishing, doi:10.1088/1742-6596/2712/1/012007.

[9] Thamir A.D., Haider A.J., Mohammed F.Q. and Chahrour K.M. (2017): *Hybrid gas phase Ti-B-C-N coatings doped with Al*.– Journal of Alloys and Compounds., vol.723, pp.368-375.

[10] Mohammed M.T., Khan Z.A. and Siddiquee A.N. (2014): *Surface modifications of titanium materials for developing corrosion behavior in human body environment: a review*.– Procedia Materials Science, vol.6, pp.1610-1618.

[11] Bottoli F., Jellesen M.S., Christiansen T.L., Winther G. and Somers M.A.J. (2018): *High temperature solution-nitriding and low-temperature nitriding of AISI 316: Effect on pitting potential and crevice corrosion performance*.– Appl. Surf. Sci. vol.431, pp.24-31, doi:https://doi.org/10.1016/j.apsusc.2017.06.094.

[12] Chen N., Ma G., Zhu W., Godfrey A., Shen Z., Wu G. and Huang X. (2019): *Enhancement of an additive-manufactured austenitic stainless steel by post-manufacture heat-treatment*.– Mater. Sci. Eng. A., vol.759, pp.65-69, doi:https://doi.org/10.1016/j.msea.2019.04.111.

[13] Visuttipitukul P., Paarai C. and Kuwahara H. (2006): *Characterization of plasma nitrided AISI H13 tool steel*.– Acta Metallurgica Slovaca, vol.12, No.3, pp.264-274.

[14] Espinoza R.C., Vera M.A., Wettlaufer M., Kerl M., Barth S., Garibaldi P.M., Guillen J.C.D., García H.M.H. Arroyo R.M. and Ortega J.A. (2024): *Study on the tribological properties of DIN 16MnCr5 Steel after duplex gas-nitriding and pack boriding*.– Materials, MDPI, vol.17, p.3057, https://doi.org/10.3390/ma17133057.

[15] Saeidi K., Gao X., Zhong Y. and Shen Z.J. (2015): *Hardened austenite steel with columnar subgrain structure formed by laser melting*.– Mater. Sci. Eng. A., vol.625, pp.221-229, doi:https://doi.org/10.1016/j.msea.2014.12.018.

[16] Wang Y. (1997): *A study of PVD coatings and die materials for extended die-casting die life*.– Surface and Coatings Technology, vol.94-95, pp.60-63, https://doi.org/10.1016/S0257-8972(97)00476-3.

[17] Fayyadh S.K. and Mohammed F.Q. (2023): *Corrosion resistance enhancement for low carbon steel by gas phase coating*.– Journal of Mechanical Engineering, vol.20, No.2, pp.139-152.

[18] Akhtar S.S., Arif A.F.M. and Yilbas B.S. (2010): *Evaluation of gas nitriding process with in-process variation of nitriding potential for AISI H13 tool steel*.– International Journal of Advanced Manufacturing Technology, vol.47, pp.687-698.

[19] Sjöström J. and Bergström J. (2004): *Thermal fatigue testing of chromium martensitic hot-work tool steel after different austenitizing treatments*.– Mater. Process Technol., vol.153-154, pp.1089-1096.

[20] Youn K.T., Rhyim Y.M, Lee J.H., Lee C.G. and Jung Y.C. (2007): *Effect of gas nitriding on the thermal fatigue behavior of martensitic chromium hot-work tool steel*.– Key Eng. Mater., vol.345-346, pp.701-704.

[21] Mohammed M.T., Lafta A.H. and Mohammed F.Q. (2023): *Surface characterization of pure and composite sol-gel nano-coatings deposited on 316L stainless steel for hard tissue replacements*.– Materials Research., vol.26, e20220479, https://doi.org/10.1590/1980-5373-MR-2022-0479.

[22] Hirsch T., Clarke T.G.R. and Rocha A.S. (2007): *An in-situ study of plasma nitriding*.– Surf. Coat. Technol., vol.201, pp.6380-6386.

[23] Cui Z.D., Zhu S.L., Man H.C. and Yang X.J. (2005): *Microstructure and wear performance of gradient Ti/TiN metal matrix composite coating synthesized using a gas nitriding technology*.– Surf. Coating. Technol., vol.190, pp.309-313.

[24] Kochmański P., Długozima M. and Baranowska J. (2022): *Structure and properties of gas-nitrided, precipitation-hardened martensitic stainless steel*.– Materials, vol.15, No.3, p.907, https://doi.org/10.3390/ ma15030907.

[25] Lisiecki A. (2015): *Titanium matrix composite Ti/TiN produced by diode laser gas nitriding*.– Metals-Basel, vol.5, pp.54-69.

[26] Xu Y.H., Zhu Z.H., Zhao H. and Zhou J. (2019): *$MoNb_{12}O_{33}$ as a new anode material for high-capacity, safe, rapid and durable Li^{+}storage: structural characteristics, electrochemical properties and working mechanisms*.– Journal of Materials Chemistry A, vol.7, No.11, p.12, https://doi.org/10.1039/rsc.

[27] Smoljan B. (2002): *AMST'02 Advanced Manufacturing Systems and Technology*.– Proceedings of the Sixth International Conference, ISBN-978-3-7091-2557-1.

[28] Vander Voort G.F., Lucas G.M. and Manilova E.P. (2004): *Metallography and microstructures of stainless steels and maraging steels*.– In: Vander Voort GF, editor. Metallogr. Microstruct. ASM International, pp.670-700, https://doi.org/10.31399/ asm.hb.v09.a0003767.

[29] Totten G.E. (2007): *Steel Heat Treatment Handbook*.– Second Edition, CRC Press, Boca Raton.

[30] Zhong Y., Liu L., Wikman S., Cui D., Shen Z. and Nucl J. (2016): *Intragranular cellular segregation network structure strengthening 316L stainless steel prepared by selective laser melting*.– Journal of Nuclear Materials, vol.470 pp.170-178, doi:10.1016/j.jnucmat.2015.12.034.

[31] Al-Saraireh F.M. and Suhymat S.A. (2024): *Effect of gas nitriding parameters on the micro-hardness of high-speed steel-cutting tools*.– Journal of Applied Engineering Science, vol.22, No.3, pp.621-633, doi:10.5937/jaes0-50375.

[32] Singh R. and Jit B. (2021): *Effect of carbide precipitation on 316L austenitic stainless steel welded joints*.– Notion Press India, ISBN: 978-1684871735.

Received: August 13, 2024
Revised: November 15, 2024